DOI: 10.1002/chem.200903404

Tuning the Magnetic Moment of $[Ru_2(DPhF)_3(O_2CMe)L]^+$ Complexes (DPhF = *N*,*N*′-Diphenylformamidinate): A Theoretical Explanation of the Axial Ligand Influence

M. Carmen Barral,[a] David Casanova,*[b] Santiago Herrero,[a] Reyes Jiménez-Aparicio,*[a] M. Rosario Torres,[c] and Francisco A. Urbanos[a]

Abstract: The magnetic behaviour of the compounds containing the $[Ru_2(DPhF)_3(O_2CMe)]^+$ ion ($DPhF^- =$ *N*,*N*′-diphenylformamidinate) shows a strong dependence on the nature of the ligand bonded to the axial position. The new complexes $[Ru_2(DPhF)_3(O_2CMe)(OPMe_3)][BF_4]\cdot 0.5\,CH_2Cl_2$ (**1**·$0.5\,CH_2Cl_2$) and $[Ru_2(DPhF)_3(O_2CMe)(4\text{-pic})][BF_4]$ (**2**) (4-pic = 4-methylpyridine) clearly display this influence. Complex **1**·$0.5\,CH_2Cl_2$ shows a magnetic moment corresponding to a $S = {}^3/_2$ system affected by the common zero-field splitting (ZFS) and a weak antiferromagnetic interaction, whereas complex **2** displays an intermediate behaviour between $S = {}^3/_2$ and $S = {}^1/_2$ systems. The experimental data of complex **1** are fitted with a model that considers the ZFS effect using the Hamiltonian $\hat{H}_D = \mathbf{S}\cdot\mathbf{D}\cdot\mathbf{S}$. The weak antiferromagnetic coupling is introduced as a perturbation, using the molecular field approximation. DFT calculations demonstrate that, in the $[Ru_2(O_2CMe)(DPhF)_3(L)]^+$ complexes, the energy level of the metal–metal molecular orbitals is strongly dependent on the nature of the axial ligand (L). This study reveals that the increase in the π-acceptor character of L leads to a greater split between the π* and δ* HOMO orbitals. The influence of the axial ligand in the relative energy between the doublet and quartet states in this type of complexes was also analysed. This study was performed on the new complexes **1**·$0.5\,CH_2Cl_2$ and **2**. The previously isolated $[Ru_2(DPhF)_3(O_2CMe)(OH_2)][BF_4]\cdot 0.5\,CH_2Cl_2$ (**3**·$0.5\,CH_2Cl_2$) and $[Ru_2(DPhF)_3(O_2CMe)(CO)][BF_4]\cdot CH_2Cl_2$ (**4**·CH_2Cl_2) complexes were also included in this study as representative examples of spin-admixed and low-spin configurations, respectively. The $[Ru_2(DPhF)_3(O_2CMe)]^+$ (**5**) unit was used as a reference compound. These theoretical studies are in accordance with the different magnetic behaviour experimentally observed.

Keywords: density functional calculations · formamidinate compounds · magnetic properties · metal–metal interactions · ruthenium

Introduction

Since the recognition of the existence of compounds that contain metal–metal multiple bonds, numerous complexes showing paddlewheel structures have been described.[1,2] Thus, examples for almost all heavier transition metals and also for some of the first-row transition metals are known.[1,2] Complexes containing a M_2^{n+} ($n = 4$ and 6) core are the most usual, although mixed valence compounds with M_2^{5+} units are also known for several metals. Complexes with M_2^{3+} and M_2^{7+} cores are very scarce, but some divanadium[3,4] and diosmium[5] species of this type have been structurally characterised. Mixed valence species are generally less stable than the species with both metal atoms in the same oxidation state (II or III). However, the complexes containing Ru_2^{5+} units are especially stable with respect to

[a] Dr. M. C. Barral, Dr. S. Herrero, Dr. R. Jiménez-Aparicio, Dr. F. A. Urbanos
Departmento de Química Inorgánica
Facultad de Ciencias Químicas, Universidad Complutense de Madrid
Ciudad Universitaria, 28040-Madrid (Spain)
Fax: (+34) 1 3944352
E-mail: reyesja@quim.ucm.es

[b] Dr. D. Casanova
Institut de Química Teòrica i Computacional (IQTCUB)
Universitat de Barcelona
Martí i Franquès 1-11, 08028 Barcelona (Spain)
Fax: (+34) 93 4021231
E-mail: davidcasanovacasas@ub.edu

[c] Dr. M. R. Torres
Centro de asistencia a la investigación de rayos X
Facultad de Ciencias Químicas, Universidad Complutense de Madrid
Ciudad Universitaria, 28040-Madrid (Spain)

Supporting information for this article is available on the WWW under http://dx.doi.org/10.1002/chem.200903404.

the reduced or oxidised Ru_2^{4+} and Ru_2^{6+} cores. This singularity makes the dimetallic complexes of ruthenium very attractive for studying their magnetic properties. From the theoretical point of view, the study of the metal–metal multiple bond is one of the challenging research targets for inorganic and physical chemists. The expected molecular orbital energy order for a dimetallic M_2^{n+} unit is $\sigma<\pi<\delta<\delta^*<\pi^*<\sigma^*$, which explains the metal–metal bond orders from 1 to 4, including the fractional bond order that occur in the most stable Ru_2^{5+} compounds.

Although several ligands have been employed to prepare the $[M_2(\mu\text{-L–L})_4)]^+$ (L–L = mononegative, bidentate ligand) family, for example, amidate, hydroxypyridinate, aminopyridinate and formamidinate; the largely most explored paddlewheel Ru_2^{5+} complexes correspond to the carboxylate derivatives.[6,7] The magnetic measurements of complexes containing the $[Ru_2(\mu\text{-}O_2CR)_4]^+$ unit show the presence of three unpaired electrons ($S=3/2$), which evidences the near degeneration of the δ^* and π^* frontier orbitals. Previous theoretical calculations[8] have also evidenced the energy inversion of these orbitals, leading to a $\sigma^2\pi^4\delta^2(\pi^*\delta^*)^3$ electronic configuration. The related reduced species $[Ru_2(\mu\text{-}O_2CR)_4]$ show the presence of two unpaired electrons ($S=1$), compatible with $\pi^{*2}\delta^{*2}$ or $\pi^{*3}\delta^{*1}$ electronic configurations, although theoretical calculations discard the second possibility.[9] Therefore, the magnetic measurements of Ru_2^{5+} and Ru_2^{4+} complexes are explained with the electronic configurations $(\pi^*\delta^*)^3$ and $\delta^{*2}\pi^{*2}$, respectively, and show the presence of an important zero-field splitting (ZFS). In addition, a moderate or important interdimer magnetic interaction, depending on the structure of the complex, has been observed in Ru_2^{5+} compounds. Also a moderate interdimer magnetic interaction in the molecular Ru_2^{4+} complexes has been observed although a stronger magnetic interaction in some polymeric species[10,11] such as $[Ru_2(O_2C(CH_2)_{10}CH_3)_4(pyz)]$ (pyz = pyrazine) or $[Ru_2(O_2CCF_3)_4(phz)]$ (phz = phenazine) is present. There is no experimental data on Ru_2^{6+} carboxylate complexes due to the instability[12] of these species, which have not been isolated[2] and no theoretical studies have been carried out. However, with the highly charged sulfate ligand, the $[Ru_2(SO_4)_4(OH_2)_2]^{2-}$ complex has been synthesised and structurally characterised.[13] Magnetic studies on caesium and potassium salts of $[Ru_2(SO_4)_4(OH_2)_2]^{2-}$ are in accordance with a $\sigma^2\pi^4\delta^1\pi^{*2}\delta^{*1}$ electronic configuration ($S=2$).[13,14]

On the other hand, the substitution of the carboxylate groups by triazenide ligands ($N_3R_2^-$) in the reduced Ru_2^{4+} species leads to diamagnetic species, such as $[Ru_2(N_3R_2)_4]$ (R = *p*-$CH_3C_6H_4$, H).[8,15] The magnetic behaviour of these complexes is in accordance with a $\sigma^2\pi^4\delta^2\pi^{*4}$ electronic configuration ($S=0$). In these complexes, the experimental results were corroborated by the corresponding theoretical analyses.[16] The air-sensitive formamidinato complexes of Ru_2^{4+} are also diamagnetic.

A more complex and interesting situation was found in the formamidinato Ru_2^{5+} complexes.[17–21] Although the tetrakis(formamidinato) complexes containing a Ru_2^{5+} unit usually present the $S=3/2$ spin system, the oxidation of these species leads to diamagnetic compounds[17,19,21] compatible with a $\sigma^2\pi^4\delta^2\delta^{*2}$ electronic configuration. However, several authors[17,22] proposed a $\pi^4\delta^2\pi^{*4}$ electronic configuration due to the very long Ru–Ru distance found in these Ru_2^{6+} species. Recent DFT calculations[23] carried out on bis(alkynil) Ru_2^{6+} compounds question that simple explanation.

The results above for diruthenium derivatives indicate the influence of the nature of the equatorial bridged ligands on the metal–metal energy levels. A strong axial ligand sensibility has also been detected in tris(formamidinato) complexes of diruthenium. In recent years, a mixed ligand complex $[Ru_2(DPhF)_3(O_2CMe)Cl]$ (DPhF$^-$ = *N*,*N*′-diphenylformamidinate) containing a carboxylate group and three donor formamidinate ligands has been described.[24] The magnetic moment of this complex[25] at room temperature is in accord with a $S=3/2$ system with the usual $(\pi^*\ \delta^*)^3$ HOMO. However, the substitution of the axial chloride by a NCS^- ligand leads to the $S=1/2$ (low spin) $[Ru_2(DPhF)_3(O_2CMe)(NCS)]$ complex,[25] which indicates a π^{*3} or $\delta^{*2}\pi^*$ electronic configuration. Similar low-spin magnetic behaviour was observed[25–27] in the Ru_2^{5+} species $[Ru_2(DPhF)_4(CN)]$, $[Ru_2\{N_3(C_6H_4\text{-}p\text{-}Me)_2\}_4(MeCN)][BF_4]$, and $[Ru_2(N_3Ph_2)_3(O_2CMe)(MeCN)_2][BF_4]$ (Ph = phenyl), although, theoretical studies on these Ru_2^{5+} complexes have not been carried out. Interestingly, other related diruthenium species with magnetic properties intermediate between the high ($S=3/2$) and low ($S=1/2$) spin states have also been reported. Experimental data indicate a rather diverse behaviour, with complexes showing a Boltzmann distribution of states, for example, $[Ru_2(p\text{-}DAniF)_4Cl]$[28] (DAniF$^-$ = *N*,*N*′-*p*-anisydylformamidinate) or $[Ru_2(DPhF)_3(O_2CMe)(OH_2)][SO_3CF_3]\cdot THF$;[29] a physical mixture of spins, for example, $[\{Ru_2(DPhF)_3(OH_2)\}_3\{1,3,5\text{-}(O_2C)_3\text{-}C_6H_3\}][SO_3CF_3]_3$;[30] or systems with quantum admixture of spins, for example, $[Ru_2(DPhF)_3(O_2CMe)(OH_2)][BF_4]\cdot 0.5\,CH_2Cl_2$.[31]

Such diversity of magnetic behaviours are usually observed in some first-row transition-metal complexes, in which high, low, and intermediate spin states are possible.[32–37] However, the examples with the second- and third-row transition metals are known only for the above-mentioned diruthenium complexes.[25,29–31,38] In some of these compounds the $S=1/2$ and $S=3/2$ spin states are sufficiently close in energy that either can be obtained by variation of the axial ligand. Therefore, it would be useful to know if the control of the spin state of these complexes is possible. The control of the spin state is a very important property to construct molecular devices useful for spintronics, for optical molecular switches, and in biological process or other applications.[39–41]

Herein, we present the synthesis, characterisation, and magnetic behaviour of two new complexes containing a Ru_2^{5+} unit, $[Ru_2(DPhF)_3(O_2CMe)(OPMe_3)][BF_4]\cdot 0.5\,CH_2Cl_2$ (**1**·0.5 CH_2Cl_2) and $[Ru_2(DPhF)_3(O_2CMe)(4\text{-pic})][BF_4]$ (**2**) (4-pic = 4-methylpyridine). In order to correlate the different types of electronic and magnetic behaviour in tris(formamidinato)diruthenium complexes with the nature of the

axial ligand, DFT with the use of the B3LYP hybrid functional calculations on **1**, **2**, and the previously reported $[Ru_2(DPhF)_3(O_2CMe)(OH_2)][BF_4]\cdot 0.5\,CH_2Cl_2$ (**3**·0.5 CH_2Cl_2),[31] and $[Ru_2(DPhF)_3(O_2CMe)(CO)][BF_4]\cdot CH_2Cl_2$ (**4**·CH_2Cl_2),[42] were carried out (Figure 1). DFT calculations on the free axial ligand cationic complex $[Ru_2(DPhF)_3(O_2CMe)]^+$ (**5**) were also carried out in order to establish a reference. Complexes **1**–**4** were chosen because they are representative examples of the variety of magnetic properties found in tris(formamidinato)diruthenium complexes. Thus, **1** and **4**·CH_2Cl_2 complexes represent the high and low spin states, respectively, and complexes **3**·0.5 CH_2Cl_2 and **2** represent two different intermediate situations.

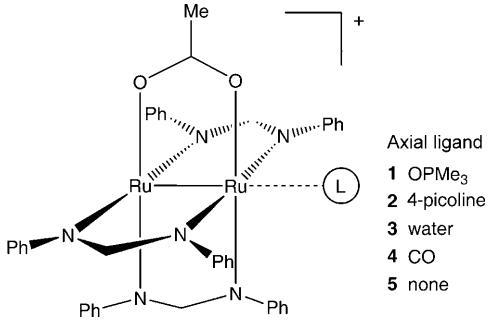

Figure 1. Geometric structure of the diruthenium studied complexes.

Results and Discussion

Synthesis of the complexes: The precipitation of silver chloride from $[Ru_2(O_2CR)_4Cl]$ or $[Ru_2(DPhF)_3(O_2CR)Cl]$ (R = alkyl or aryl) with silver salts leads to the corresponding cationic complexes.[25,30,38,43] The addition of 4-pic to a solution of the cationic species $[Ru_2(DPhF)_3(O_2CMe)]^+$ gives **1**. In a similar reaction with PMe_3, the phosphane ligand is oxidised to $OPMe_3$ which is coordinated in the axial position to form **2**.

The infrared (IR) spectra of **1** and **2** show the characteristic bands due to the fragment $[Ru_2(DPhF)_3(O_2CMe)]^+$ and corresponding to the BF_4^- ion.[30] Complex **1** also shows an additional band at 1143 cm^{-1} assigned to the stretching vibration of the O=PMe_3 bond, which has been reported for the uncoordinated ligand at slightly lower than 1163 cm^{-1}.[44] In the IR spectrum of **2**, overlapping bands at 1619 and 809 cm^{-1} due to the dimetallic fragment can be assigned to the 4-picoline ligand, which appear at 1608 and 803 cm^{-1} in the free ligand.[45]

X-ray structure determinations: Crystal data of complexes $[Ru_2(DPhF)_3(O_2CMe)(OPMe_3)][BF_4]\cdot 0.5\,CH_2Cl_2$ (**1**·0.5 CH_2Cl_2) and $[Ru_2(DPhF)_3(O_2CMe)(4\text{-pic})][BF_4]$ (**2**) are collected in Table 1. Both cationic complexes adopt the typical paddlewheel structure described for numerous Ru_2^{5+} compounds (Figures 2 and 3). In both cases, only one of the axial positions is occupied by the neutral ligand, which have

Table 1. Crystallographic data for $[Ru_2(DPhF)_3(O_2CMe)(OPMe_3)][BF_4]\cdot 0.5\,CH_2Cl_2$ (**1**·0.5 CH_2Cl_2) and $[Ru_2(DPhF)_3(O_2CMe)(4\text{-pic})][BF_4]$ (**2**)

	1·0.5 CH_2Cl_2	**2**
formula	$C_{89}H_{92}B_2Cl_2F_8N_{12}O_6P_2Ru_4$	$C_{47}H_{43}BF_4N_7O_2Ru_2$
M_r	2136.49	1026.83
crystal system	monoclinic	monoclinic
space group	$P21/c$	$P21/n$
a [Å]	13.5806(8)	11.5639(7)
b [Å]	17.727(1)	17.097(1)
c [Å]	39.221(2)	23.292(1)
β [°]	98.838(1)	104.370(1)
V [Å^3]	9330.3(9)	4460.9(5)
Z	4	4
ρ_{calcd} [g cm^{-3}]	1.521	1.529
μ [mm^{-1}]	0.801	0.741
$F(000)$	4320	2076
crystal size [mm^3]	0.05×0.11×0.28	0.12×0.18×0.24
θ range [°]	1.05–25.00	1.49–26
index ranges	$-10\le h\le 16$ $-21\le k\le 21$ $-46\le l\le 44$	$-12\le h\le 14$ $-21\le k\le 20$ $-28\le l\le 24$
reflns collected	48362	24974
independent reflns	16423 [R_{int} = 0.1053]	8736 [R_{int} = 0.0682]
completeness [%] to θ = max	99.9	91.2
absorption correction	none	none
data/restraints/parameters	16423/10/1012	10775/4/538
GOF on F^2	1.004	1.001
R[a]	0.0664	0.0524
R_{wF}[b]	0.1793	0.1680

[a] $\Sigma||F_o|-|F_c||/\Sigma|F_o|$. [b] $\{\Sigma[w(F_o^2-F_c^2)^2]/\Sigma[w(F_o^2)^2]\}^{1/2}$

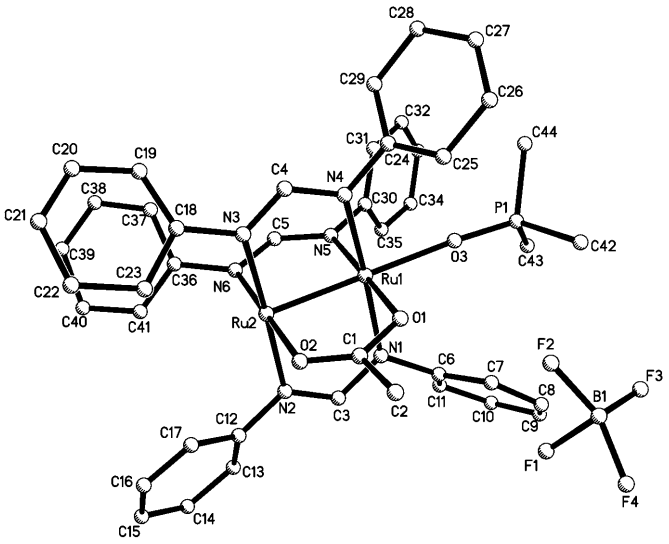

Figure 2. ORTEP diagram of one $Ru_2(DPhF)_3(O_2CMe)(OPMe_3)][BF_4]$ unit of complex **1**·0.5 CH_2Cl_2. Ellipsoids are drawn at 20% probability. Hydrogen atoms are omitted for clarity.

already been observed for the complexes $[Ru_2(DPhF)_3(O_2CMe)(OH_2)][BF_4]\cdot 0.5\,CH_2Cl_2$ (**3**·0.5 CH_2Cl_2) and $[Ru_2(DPhF)_3(O_2CMe)(CO)][BF_4]\cdot CH_2Cl_2$ (**4**·CH_2Cl_2). Selected geometric parameters of compounds **1**·0.5 CH_2Cl_2 and **2** are provided in Table 2. Geometric parameters for complexes **3**

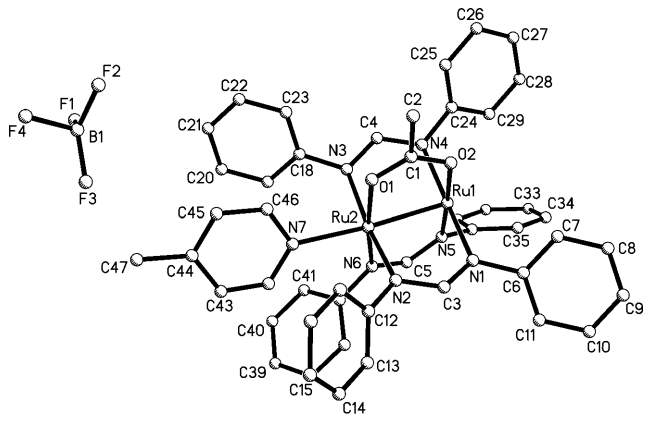

Figure 3. ORTEP diagram of $[Ru_2(DPhF)_3(O_2CMe)(4\text{-pic})][BF_4]$ (**2**). Ellipsoids are drawn at 20% probability. Hydrogen atoms are omitted for clarity.

and **4** are also collected for comparison purpose. It is worth noting the increase of the Ru–Ru bond length (ca. 0.15 Å) from complex **1**·0.5 CH_2Cl_2 to **4**·CH_2Cl_2. This elongation is ascribed to the increase of the π-acceptor character of the axial ligand which rises from the π donor $OPMe_3$ group in complex **1** to the strong π acceptor CO molecule in **4**.

In complex **1**·0.5 CH_2Cl_2, there are two independent dimetal cations in the unit cell. Although both of them have the same metal–metal distance (2.302 Å), other equivalent bond lengths are significantly different: Ru1–O3 = 2.124 and Ru3–O6 = 2.151 Å; Ru1–O1 = 2.049 and Ru3–O4 = 2.081 Å; Ru2–O2 = 2.072 and Ru4–O5 = 2.055 Å. The cations are essentially eclipsed in the first case and slightly rotated in the second, as illustrated by the following torsion angles: O1-Ru1-Ru2-O2 = −1.3° and O4-Ru3-Ru4-O5 = 4.2°.

Table 2. Characteristic structural parameters of $[Ru_2(DPhF)_3(O_2CMe)L]^+$ ions. Ru–Ru and Ru–L atomic distances [Å], Ru-Ru-L angle, and O-Ru-Ru-O dihedral angle [°].[a]

	Complex	Ru–Ru	Ru–L	Ru-Ru-L	O-Ru-Ru-O
1a	$[Ru_2(DPhF)_3(O_2CMe)(OPMe_3)]^+$	2.303	2.125	178.5	1.3
1b	$[Ru_2(DPhF)_3(O_2CMe)(OPMe_3)]^+$	2.302	2.151	179.1	4.2
2	$[Ru_2(DPhF)_3(O_2CMe)(4\text{-pic})]^+$	2.408	2.274	172.1	5.1
3a	$[Ru_2(DPhF)_3(O_2CMe)(H_2O)]^+$	2.350	2.343	171.9	0.3
3b	$[Ru_2(DPhF)_3(O_2CMe)(H_2O)]^+$	2.350	2.339	178.3	0.3
4	$[Ru_2(DPhF)_3(O_2CMe)(CO)]^+$	2.450	2.032	176.0	0.7
5	$[Ru_2(DPhF)_3(O_2CMe)]^+$		2.283		1.6

[a] The **a** and **b** labels indicate different crystallographic sites.

Magnetic properties: The magnetic susceptibility of complexes **1**·0.5 CH_2Cl_2 and **2** increases with a decrease in temperature. The magnetic moment value, at room temperature, for **1**·0.5 CH_2Cl_2 is 3.89 μ_B in accordance with a $S = {}^3/_2$ system, and decreases with the temperature until 2.91 μ_B, near to the corresponding spin for two unpaired electrons. The decrease of the magnetic moment with the temperature observed for complex **1** is typical for high-spin Ru_2^{5+} compounds and has been ascribed to an important ZFS together with small antiferromagnetic interactions among the dimetallic units. The ZFS effect on the susceptibility can be quantified by considering the Hamiltonian $\hat{H}_D = \mathbf{S}\cdot\mathbf{D}\cdot\mathbf{S}$ as described by O'Connor [Eqs. (1)–(3)].[46] A temperature-independent paramagnetism term (TIP) is added to the ZFS system, and the weak antiferromagnetic coupling was considered by using the molecular field approximation [Eqs. (4) and (5)] .[46] In addition, the presence of a small quantity of paramagnetic impurity (P) [Eq. (6)] was taking into account.

$$\chi_{\parallel} = \frac{Ng^2\beta^2}{k\mathrm{T}} \frac{1 + 9\, e^{\frac{-2D}{kT}}}{4\left(1 + e^{\frac{-2D}{kT}}\right)} \tag{1}$$

$$\chi_{\perp} = \frac{Ng^2\beta^2}{k\mathrm{T}} \frac{\left(4 + \frac{3kT}{D}\right)\left(1 + 9e^{\frac{-2D}{kT}}\right)}{4\left(1 + e^{\frac{-2D}{kT}}\right)} \tag{2}$$

$$\chi_{\mathrm{M}} = \frac{\chi_{\parallel} + 2\chi_{\perp}}{3} \tag{3}$$

$$\chi'_{\mathrm{M}} = \chi_{\mathrm{M}} + \mathrm{TIP} \tag{4}$$

$$\chi' = \frac{\chi'_{\mathrm{M}}}{1 - \left(\frac{2zJ}{Ng^2\beta^2}\right)\chi'_{\mathrm{M}}} \tag{5}$$

$$\chi'_{\mathrm{mol}} = (1-P)\chi' + P\frac{Ng^2\beta^2}{4kT} \tag{6}$$

The fit of the experimental data using Equation (6) leads to g, D, J, TIP, and P values of 2.03, 51.17 cm^{-1}, −0.05 cm^{-1}, 2.96 10^{-9} emu mol^{-1}, and 0.04%, respectively (Figure 4), which are similar to those found in other analogous diruthenium complexes.[47–50] Complex **2** displays a magnetic susceptibility curve very different from that described for **1**. Thus, the room-temperature magnetic moment of 2.86 μ_B is lower than the expected for a $S = {}^3/_2$ system, and it decreases with the temperature to 1.98 μ_B, corresponding to a $S = {}^1/_2$ system. In addition, the variation of the magnetic moment curve versus temperature is almost linear (Figure 5), which indicates that the observed decrease is not due to ZFS or antiferromagnetic interactions. An almost linear variation of the magnetic moment with the temperature has been also described for $[Ru_2(DPhF)_3(O_2CC_6F_5)(OH_2)_2][SO_3CF_3]$ and $[Ru_2(DPhF)_3(O_2CMe)(OH_2)][BF_4]$·0.5 CH_2Cl_2, which show a spin-admixed behaviour.[31,38] The magnetic moment curves for all of the complexes studied in this work are collected in Figure 5. In the composition of the cation complexes corre-

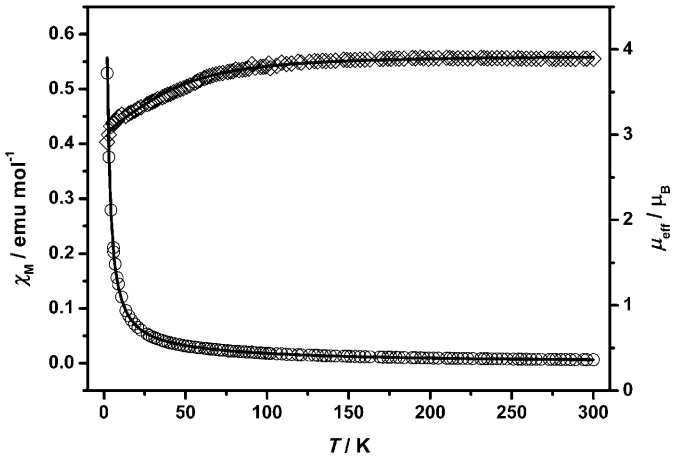

Figure 4. Dependence of the magnetic susceptibility (○) and moment (◇) on the temperature for $[Ru_2(DPhF)_3(O_2CMe)(OPMe_3)][BF_4]\cdot 0.5\,CH_2Cl_2$ (**1**·0.5 CH_2Cl_2). Solid lines are the result to fit the experimental data using the model mentioned in the text.

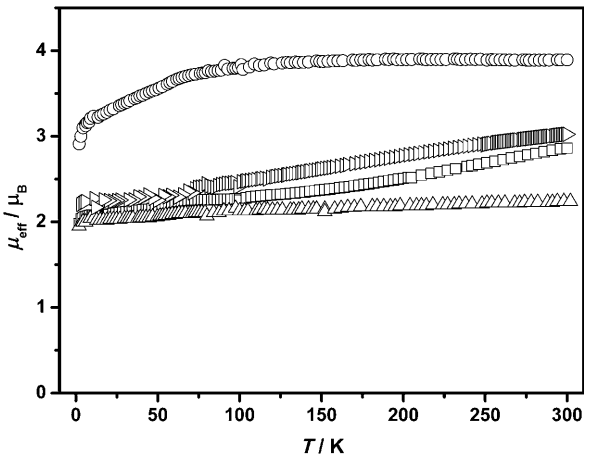

Figure 5. Magnetic moment curves versus temperature for $[Ru_2(DPhF)_3(O_2CMe)(OPMe_3)][BF_4]\cdot 0.5\,CH_2Cl_2$ (**1**·0.5 CH_2Cl_2) (○), $[Ru_2(DPhF)_3(O_2CMe)(H_2O)][BF_4]\cdot 0.5\,CH_2Cl_2$ (**3**·0.5 CH_2Cl_2) (▷), $[Ru_2(DPhF)_3(O_2CMe)(4\text{-pic})][BF_4]$ (**2**) (□), and $[Ru_2(DPhF)_3(O_2CMe)(CO)][BF_4]\cdot CH_2Cl_2$ (**4**·CH_2Cl_2) (△).

sponding to the compounds **1**–**4**, the only difference is the axial ligand and, therefore, the different nature of these ligands seems mainly to be responsible for the changes observed in the magnetic properties.

Computational study: The energy ordering of the Ru_2^{n+} molecular orbitals (MO), described using the traditional metal–metal bond model, is not so evident if one takes into account the interaction of the dimetallic unit with the coordinated ligands. Previous studies[9] on $[Ru_2(O_2CMe)_4]^+$ showed how the more efficient destabilisation of the δ* orbital, owing to antibonding interactions with the $1b_u$ carboxylate orbitals, gives a final electronic configuration associated with $\sigma\pi\delta\pi^*\delta^*\sigma^*$ orbital energy ordering. The replacement of three carboxylate ligands by the more donating group $DPhF^-$ in reference complex $[Ru_2(DPhF)_3(O_2CMe)]^+$ (**5**) does not change the $\pi^* < \delta^*$ energy order and an even further destabilisation of the latter might be expected. On the other hand, the presence of a π-acid ligand in the axial coordination site of $[Ru_2(O_2CMe)_4(L)]^+$ (L = pyrazine or pyridine) is able to reverse the energy order of HOMO orbitals.[7] This situation is more unlikely to happen in the $[Ru_2(DPhF)_3(O_2CMe)(L)]^+$ compounds due to the stronger δ* destabilisation.

Probably the key factor in the determination of the ground-state spin multiplicity of $[Ru_2(DPhF)_3(O_2CMe)(L)]^+$ compounds, doublet ($S = {}^1/_2$) or quartet ($S = {}^3/_2$) electronic configuration, is the magnitude of the energy separation between the π* and δ* frontier orbitals. Since it is reflected in the magnetic experimental data, the axial ligand (L) plays a crucial role in the preferred multiplicity. In order to comprehend how L tunes the electronic structure of this family, we have chosen the energy of the optimised ligand-free complex $[Ru_2(DPhF)_3(O_2CMe)]^+$ (**5**) as reference. Taking **5** as a zero-order approximation to the $[Ru_2(DPhF)_3(O_2CMe)(L)]^+$ electronic structure and analysing how it is perturbed by L, it will be a rather natural and straightforward manner to rationalise the role of the studied ligands.

Although the molecular orbital energies do not allow for the direct knowledge of the total energy of any system, the use of a molecular orbital energy diagram for the compounds **1**–**4** gives a qualitative understanding of the doublet/quartet relative stability in the $[Ru_2(DPhF)_3(O_2CMe)(L)]^+$ family. Figure 6 shows the molecular orbital diagram calculated for each complex for both possible configurations, doublet and quartet, on the left and the right sides of the dashed line, respectively. Energies are referenced to the δ* energy orbital of the quartet state [$E(\delta^*) = 0$ eV], due the near invariability of the split between the δ and δ* orbitals in this state. The change in the spin multiplicity is caused by

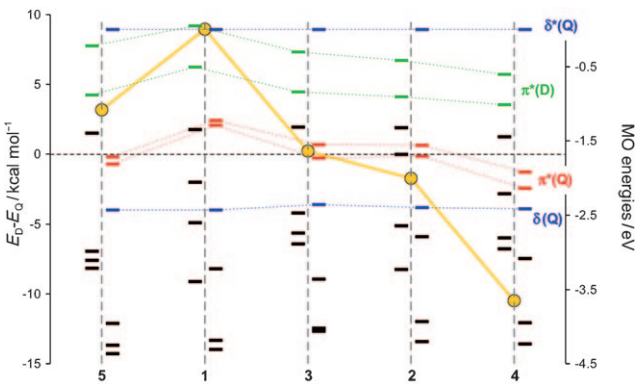

Figure 6. α-Spin orbital diagram of the doublet (left of the dashed line) and quartet (right of the dashed line) states for **1**–**5**. Energies are relative to the δ* (quartet) orbital energy considered as zero. For clarity, molecular orbitals in the same range of energy and with large contributions of atomic orbitals coming from the equatorial ligands are not presented in the diagram, and only the results for **1a** and **3b** are presented for these species. Coloured orbitals correspond to $S = {}^3/_2$ state δ*(Q), δ(Q) (blue) and π*(Q) (red) and $S = {}^1/_2$ state π* (D) (green). The yellow line represents the energy difference between the doublet and quartet states.

the transfer of one electron from the π* (doublet) to the δ* (quartet) orbitals or vice versa. Thus, the relative energy of the highest occupied π* orbitals in the doublet state with respect to the δ* orbital of the quartet state can be qualitatively associated to the spin preference. The gap between π* and δ* levels and, therefore, the low spin state stability increase in the order **1**·0.5 CH_2Cl_2 < **3**·0.5 CH_2Cl_2 < **2** < **4**·CH_2Cl_2 from compounds **1** to **4**. In this order there is an increase of the gap between π* and δ* levels, which increases the stability of the low spin state. However, care must be taken when trying to draw quantitative conclusions from the magnitude of the molecular orbital energy gaps obtained from DFT calculations[51,52], especially when hybrid functionals (like B3LYP) are used.

The energies of the quartet and doublet states were also calculated in order to know the preferred electronic state for each complex. The calculations carried out on the fully optimised **5** show a preference of the quartet state over the doublet state by 3.18 kcal mol^{-1}. The energies of both states, for complexes **1**–**4**, were determined using the experimental atomic positions. In Figure 6 (yellow line), the differences between the energy of the doublet and quartet states are shown. It can be observed that the quartet state for complex **1** is more stable than for the reference species **5** by about 8.5 kcal mol^{-1}. In contrast, the doublet state in **4** is lower in energy than the quartet state (10.49 kcal mol^{-1}). These calculations are in accordance with the magnetic behaviour described above for these compounds. Complexes **2** and **3** show the quartet and doublet states as ground states, respectively. However, in these cases, the energy difference between both states is lower than 2 kcal mol^{-1}, which allows thermal access to the excited state. As a consequence, a magnetic intermediate response between high and low spin is expected. These expectations are in accordance with the above mentioned experimental magnetic data. Thus, the coordination of an axial ligand L to the complex results in a non-negligible perturbation of the electronic structure, which can favour either the quartet or the doublet state

Additionally, there seems to be a direct relationship between the donor/acceptor character of the axial ligand and the Ru–Ru distance. Those ligands more capable of giving electronic density to the frontier dimetallic antibonding orbitals will induce larger interatomic distances. At the same time, the destabilisation due to shorter Ru–Ru separation affects δ* and π* orbitals differently. While the δ interactions at the Ru–Ru experimental distances (2.30–2.45 Å) are expected to be rather weak, the π* orbitals are much more sensitive to changes of the dimetallic separation. Shorter distances destabilise the π*, reducing the gap to δ* and, thus, stabilising the quartet versus the doublet state (Figure 7).

From simple symmetry considerations, it can be assumed that the presence of the explored axial ligands (trimethylphosphane oxide, water, 4-picoline and carbonyl) does not directly change the characteristics of the δ and δ* orbitals and they will only be indirectly modified through molecular geometry variations. It becomes clear since the δ–δ* energy

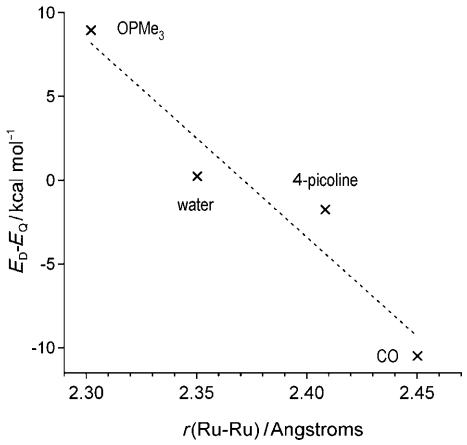

Figure 7. Computed quartet to doublet energy gap [kcal mol^{-1}] versus Ru–Ru interatomic distance [Angstroms].

gap is similar for all of the complexes studied (Figure 6). On the other hand, this behaviour is not observed in σ- and π-symmetry orbitals. Both the doubly occupied σ and the virtual σ* are strongly destabilised by the antibonding interactions with the axial ligand. Destabilisation of π-symmetry orbitals is much more variable, since it depends on the π-donor or π-acceptor characteristics of L (see below).

The weak σ-donor character of H_2O and $OPMe_3$ ligands in $[Ru_2(DPhF)_3(O_2CMe)(H_2O)]^+$ and $[Ru_2(DPhF)_3(O_2CMe)(OPMe_3)]^+$ results in relatively small increases in the Ru–Ru distances, 2.350 and 2.302 Å, respectively, versus complex **5** (2.283 Å). In addition to the $(\sigma–\sigma_L)^*$ and $(\sigma^*–\sigma_L)^*$ destabilisation, which is common in **1**–**4**, the antibonding interaction of the oxygen p orbital of $OPMe_3$ with π* further pushes its energy level towards δ* (Figure 8), increasing the relative stabilisation of the quartet state. In fact, compound **1**·0.5 CH_2Cl_2 represents the largest quartet to doublet energy difference in the **1**–**4** complexes, which agrees with the experimental effective magnetic moment measures (Table 3 and Figures 4, 5, and 9). The results of energy calculations for the doublet and quartet states in

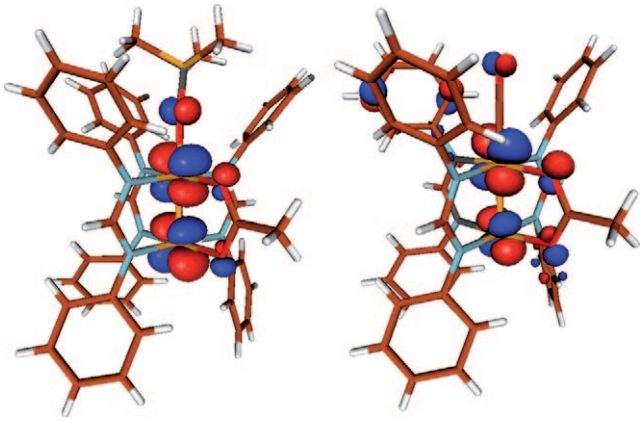

Figure 8. Representation of the highest energy singly occupied π* molecular orbitals in $[Ru_2(DPhF)_3(O_2CMe)(OPMe_3)]^+$ (left) and $[Ru_2(DPhF)_3(O_2CMe)(CO)]^+$ (right), contour value cutoff = 0.05 e bohr^{-3}.

Table 3. Ru–Ru atomic distances, experimental effective magnetic moments at room temperature and quartet to doublet energy gaps of the $[Ru_2(DPhF)_3(O_2CMe)L]^+$ studied compounds.

	Complex	d_{Ru-Ru} [Å]	μ_{eff} [μ_B]	E_D-E_Q [kcal mol^{-1}]
1a	$[Ru_2(DPhF)_3(O_2CMe)(OPMe_3)]^+$	2.303	3.89	8.87
1b	$[Ru_2(DPhF)_3(O_2CMe)(OPMe_3)]^+$	2.302	3.89	8.28
2	$[Ru_2(DPhF)_3(O_2CMe)(4\text{-pic})]^+$	2.408	2.86	−1.76
3a	$[Ru_2(DPhF)_3(O_2CMe)(H_2O)]^+$	2.350	3.09[a]	0.23
3b	$[Ru_2(DPhF)_3(O_2CMe)(H_2O)]^+$	2.350	3.09[a]	0.60
4	$[Ru_2(DPhF)_3(O_2CMe)(CO)]^+$	2.450	2.03[b] 2.24[c]	−10.49
5	$[Ru_2(DPhF)_3(O_2CMe)]^+$	2.283		3.18

[a] From reference [31]. [b] Experimental magnetic moments of **4** were measured as $[Ru_2(DPhF)_3(O_2CMe)(CO)][BF_4]$ crystallised in CH_2Cl_2.[42] [c] Experimental magnetic moments of **4** were measured as $[Ru_2(DPhF)_3(O_2CMe)(CO)][BF_4]$ crystallised in THF.[42]

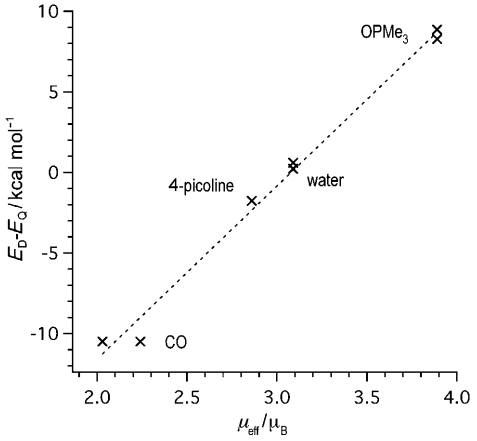

Figure 9. Computed quartet to doublet energy gap [kcal mol^{-1}] versus experimental effective magnetic moments [B.M.], at room temperature.

$[Ru_2(DPhF)_3(O_2CMe)(4\text{-pic})]^+$ show a slight preference for the lower multiplicity by 1.76 kcal mol^{-1}. The larger σ-donor character of picoline ligand, compared to, for instance, the water ligand in complex **3**, causes a quite high $(\sigma-\sigma_L)^*$ orbital destabilisation. Finally, the axial coordination of CO induces a preference for the low spin state by 10.49 kcal mol^{-1}. This computed gap is in agreement with experimental magnetic measurements[42] that indicate one unpaired electron and a paramagnetic ground state for a wide temperature range. The main reason for can be found in the π-acceptor nature of CO, which is able to stabilise the π* orbitals (Figure 6) and increases the δ* orbital gap.

Conclusion

Density functional theory computations on the new **1**·0.5 CH_2Cl_2 and **2**, and the previously experimentally studied **3**·0.5 CH_2Cl_2 and **4**·CH_2Cl_2 diruthenium compounds were able to improve the understanding of the ground state electronic structure nature of the $[Ru_2(DPhF)_3(O_2CMe)L]^+$ family. The trend of computed quartet to doublet energy gap is in good agreement with experimental magnetic measurements. The calculated energy gap can be qualitatively rationalised by the δ* to π* energy difference which can be tuned by the nature of the axial ligand. The $[Ru_2(DPhF)_3(O_2CMe)]^+$ complex gives a zero-order approximation to the electronic structure of the general $[Ru_2(DPhF)_3(O_2CMe)L]^+$ family. This can be thereafter perturbed by the choice of different coordinated axial ligands, modifying the electronic properties almost at will. The π-donor or π-acceptor properties of the axial ligands were shown to be crucial in the stability of the possible spin multiplicities, doublet or quartet spin sates. These results open the door to the preparation of other diruthenium complexes using different donor/acceptor equatorial and axial ligands to achieve a desired spin value.

The simple methodology employed in this study can be easily extended to other similar compounds, of which the magnetic properties also present anomalous behaviour. The inclusion of spin-orbital coupling in the computation allows for a direct comparison of computed quartet-doublet energy gaps to experimental variable temperature magnetic measurements.

Experimental Section

Materials and equipment: All of the reactions were carried out in air. Chemicals and solvents were purchased from commercial sources and used without further purification. Compounds $[Ru_2(DPhF)_3(O_2CMe)(OH_2)][BF_4]$·0.5 CH_2Cl_2 (**3**·0.5 CH_2Cl_2) and $[Ru_2(DPhF)_3(O_2CMe)(CO)][BF_4]$·$CH_2Cl_2$ (**4**·CH_2Cl_2) were obtained by the following published procedures.[31,42] Elemental analyses were done by the Microanalytical Service of the Complutense University of Madrid. IR spectra were obtained with a FT Midac prospect spectrophotometer using KBr pellets. Electronic spectra of the complexes in the solid state (Nujol suspension between polyethylene sheets) were acquired on a Cary 5G spectrophotometer. Variable-temperature magnetic susceptibility measurements were performed on a Quantum Design MPMS*XL* SQUID magnetometer. All data were corrected for the diamagnetic contribution to the susceptibility of both the sample holder and the compound. Molar diamagnetic corrections were calculated on the basis of Pascal's constants.

Synthesis of $[Ru_2(DPhF)_3(O_2CMe)(OPMe_3)][BF_4]$·0.5 CH_2Cl_2 (1·0.5 CH_2Cl_2): PMe_3 (0.25 mL of a 1 M solution in toluene) was added to a solution of $[Ru_2(DPhF)_3(O_2CMe)(OH_2)][BF_4]$ (0.200 g, 0.21 mmol) in dichloromethane (20 mL) and the mixture was stirred for 3.5 h. The volatile components were removed under vacuum and the residue was washed with diethyl ether (4×5 mL) and dried. The compound was recrystallised in dichloromethane/hexane. Yield: 0.14 g (62%). IR (KBr): $\tilde{\nu}$ = 3058 (vw), 1592 (m), 1536 (vs), 1488 (vs), 1439 (m), 1318 (s), 1219 (s), 1143 (s), 1083 (s), 1055 (s), 940 (m), 782 (w), 762 (m), 697 (s), 515 (w), 509 (w), 448 (w), 422 cm^{-1} (w); Vis/NIR (Nujol): λ = 490 (sh), 574, 670 nm (sh); μ_{eff} at RT: 3.89 μ_B; elemental analysis calcd (%) for $C_{44.5}H_{46}BClF_4N_6O_3Ru_2$: C 50.03, H 4.34, N 7.87; found: C 49.86, H 4.30, N 7.85.

Synthesis of $[Ru_2(DPhF)_3(O_2CMe)(4\text{-pic})][BF_4]$ (2): 4-Pic (30 μL, 0.31 mmol) was added to a bluish solution of $[Ru_2(DPhF)_3(O_2CMe)(OH_2)][BF_4]$ (0.200 g, 0.21 mmol) in dichloromethane (5 mL). The colour of the solution changed immediately to purple. The solution was stirred for 4 h and evaporated to dryness. The residue was redissolved in dichloromethane (2.5 mL) and the compound was precipitated by addition of a mixture of diethyl ether (20 mL) and hexane (20 mL). The solid was filtered and washed with diethyl ether (2×5 mL) and dried under vacuum. Yield: 0.17 g (79%). IR (KBr): $\tilde{\nu}$ = 3057 (vw), 2951 (vw), 1619

(w), 1591 (m), 1523 (s), 1487 (vs), 1447 (m), 1420 (m), 1358 (w), 1318 (s), (1212 (s), 1051 (s), 937 (m), 809 (w), 762 (s), 696 (s), 533 (w), 518 (w), 497 (w), 454 (m), 445 cm^{-1} (m); Vis/NIR (Nujol): $\lambda = 490$ (sh), 585, 720 nm (sh); MS-ESI$^+$ ($CHCl_3$): m/z (%): 848 (100) [M^+−4-pic]; μ_{eff} at RT: 2.86 μ_B; elemental analysis calcd (%) for $C_{47}H_{43}BF_4N_7O_2Ru_2$: C 54.98, H 4.22, N,9.55; found: C 54.76, H 4.27, N 9.34.

X-ray data collection and structure refinement: Suitable crystals for X-ray determination of **1**·0.5 CH_2Cl_2 and **2** were obtained by slow diffusion of hexane into solutions of the complexes in dichloromethane. Data collection (ϕ and ω scans) for both compounds was carried out at room temperature on a Bruker Smart CCD diffractometer using graphite-monochromated $Mo_{K\alpha}$ radiation ($\lambda = 0.71073$ Å) operating at 50 kV and 30 mA for **1**·0.5 CH_2Cl_2 and 50 kV and 20 mA for **2**. The data were collected over a hemisphere of the reciprocal space by combination of three exposure sets, each exposure was for 20 s for **1**·0.5 CH_2Cl_2 and 30 s for **2**, covered 0.3° in ω. The first 50 frames were recollected at the end of the data collection to monitor crystal decay. A summary of the fundamental crystal and refinement data is given in Table 1.

The structures were solved by direct methods and refined by blocked full-matrix for **1**·0.5 CH_2Cl_2 and full-matrix for **2** least-square procedures on F^2.[53] All non-hydrogen atoms were refined anisotropically with some exceptions. In both cases, the BF_4^- group was isotropically refined three cycles and, for the last cycle, the thermal factors were fixed using geometrical restraints and variable common B−F distances. The compound **1**·0.5 CH_2Cl_2 presents two molecules in the asymmetric unit and one molecule of dichloromethane from crystallisation which was refined, again, two cycles isotropically and one last cycle with the thermal factors fixed using geometrical restraints and variable common C−Cl distances. Also, some rings in **1**·0.5 CH_2Cl_2 were refined using rigid body restrains. All hydrogen atoms in **1**·0.5 CH_2Cl_2 and **2** were included in their calculated positions and refined riding on the respective carbon atoms.

CCDC-747757 (**1**) and 747758 (**2**) contain the supplementary crystallographic data for this paper. These data can be obtained free of charge from The Cambridge Crystallographic Data Centre via www.ccdc.cam.ac.uk/data_request/cif.

Computational details: Electronic structure studies of the $[Ru_2(DPhF)_3(O_2CMe)L]^+$ family (**1**–**4**) were carried out using experimental crystallographic data.[31,42] In the water complex **3**, the two non-equivalent axial coordination sites were experimentally considered[31] and were also computationally explored. The atomic positions of the two aqueous hydrogen atoms were not experimentally resolved and thus they were optimised keeping the rest of the molecule frozen to the experimental geometry. The molecular geometry of the axial ligand free $[Ru_2(DPhF)_3(O_2CMe)]^+$ complex (**5**) was fully optimised.[54] The main structural parameters of **1**–**5** are presented in Table 2. The Stuttgart RSC 1997 effective core potential (ECP)[55] was used for ruthenium atoms, an ECP for the description of the [Ar]+3d inner electrons and 6s, 5p, 3d contracted Gaussian functions to explicitly treat the valence electrons. The 6–311G* basis set from Pople[56] has been used for the rest of atoms. The above basis sets were employed in both, energy and geometry optimisation calculations in conjunction with the B3LYP[57] functional and in the framework of density functional theory (DFT). All calculations were performed with the Q-Chem program.[58]

Acknowledgements

We are grateful to Ministerio de Ciencia e Innovación (MICINN), Comunidad de Madrid (CM) and Universidad Complutense de Madrid (UCM) (projects no. CTQ2008-00920, S2009/MAT-1467, and UCM-921073-5220256) for financial support. D.C. thanks the MICINN for its financial support (RYC-2008-0223).

[1] F. A. Cotton, R. A. Walton, *Multiple Bonds between Metal Atoms*, Wiley, New York, **1982**.
[2] F. A. Cotton, C. A. Murillo, R. A. Walton, *Multiple Bonds between Metal Atoms*, Springer, New York, **2005**.
[3] F. A. Cotton, E. A. Hillard, C. A. Murillo, *J. Am. Chem. Soc.* **2003**, *125*, 2026–2027.
[4] F. A. Cotton, E. A. Hillard, C. A. Murillo, X. Wang, *Inorg. Chem.* **2003**, *42*, 6063–6070.
[5] F. A. Cotton, N. S. Dalal, P. Huang, C. A. Murillo, A. C. Stowe, X. Wang, *Inorg. Chem.* **2003**, *42*, 670–672.
[6] M. A. S. Aquino, *Coord. Chem. Rev.* **1998**, *170*, 141–202.
[7] M. A. S. Aquino, *Coord. Chem. Rev.* **2004**, *248*, 1025–1045.
[8] J. G. Norman, G. E. Renzoni, D. A. Case, *J. Am. Chem. Soc.* **1979**, *101*, 5256–5267.
[9] G. Estiú, F. D. Cukiernik, P. Maldivi, O. Poizat, *Inorg. Chem.* **1999**, *38*, 3030–3039.
[10] L. Bonnet, F. D. Cukiernik, P. Maldivi, A. M. Giroud-Godquin, J. C. Marchon, M. Ibn-Elhaj, D. Guillon, A. Skoulios, *Chem. Mater.* **1994**, *6*, 31–38.
[11] H. Miyasaka, R. Clerac, C. S. Campos-Fernandez, K. R. Dunbar, *J. Chem. Soc. Dalton Trans.* **2001**, 858–861.
[12] F. A. Cotton, M. Matusz, B. Zhong, *Inorg. Chem.* **1988**, *27*, 4368–4372.
[13] I. V. Kuzmenko, A. N. Zhilyaev, T. A. Fomina, M. A. Poraikoshits, I. B. Baranovskii, *Zh. Neorg. Khim.* **1989**, *34*, 2548–2553.
[14] A. N. Zhilyaev, T. A. Fomina, I. V. Kuzmenko, A. V. Rotov, I. B. Baranovskii, *Zh. Neorg. Khim.* **1989**, *34*, 948–952.
[15] F. A. Cotton, M. Matusz, *J. Am. Chem. Soc.* **1988**, *110*, 5761–5764.
[16] F. A. Cotton, X. Feng, *Inorg. Chem.* **1989**, *28*, 1180–1183.
[17] J. L. Bear, B. Han, S. Huang, K. M. Kadish, *Inorg. Chem.* **1996**, *35*, 3012–3021.
[18] C. Lin, T. Ren, E. J. Valente, J. D. Zubkowski, *J. Organomet. Chem.* **1999**, *579*, 114–121.
[19] G. Xu, T. Ren, *Inorg. Chem.* **2001**, *40*, 2925–2927.
[20] F. A. Cotton, T. Ren, *Inorg. Chem.* **2002**, *41*, 3190–3193.
[21] P. Angaridis, F. A. Cotton, C. A. Murillo, D. Villagran, X. Wang, *Inorg. Chem.* **2004**, *43*, 8290–8300.
[22] F. A. Cotton, A. Yokochi, *Inorg. Chem.* **1997**, *36*, 567–570.
[23] I. P.-C. Liu, T. Ren, *Inorg. Chem.* **2009**, *48*, 5608–5610.
[24] M. C. Barral, S. Herrero, R. Jiménez-Aparicio, M. R. Torres, F. A. Urbanos, *Inorg. Chem. Commun.* **2004**, *7*, 42–46.
[25] M. C. Barral, R. Gonzalez-Prieto, S. Herrero, R. Jimenez-Aparicio, J. L. Priego, E. C. Royer, M. R. Torres, F. A. Urbanos, *Polyhedron* **2004**, *23*, 2637–2644.
[26] F. A. Cotton, L. R. Falvello, T. Ren, K. Vidyasagar, *Inorg. Chim. Acta* **1992**, *194*, 163–170.
[27] F. A. Cotton, A. Yokochi, *Inorg. Chem.* **1998**, *37*, 2723–2728.
[28] P. Angaridis, F. A. Cotton, C. A. Murillo, D. Villagran, X. Wang, *J. Am. Chem. Soc.* **2005**, *127*, 5008–5009.
[29] F. A. Cotton, S. Herrero, R. Jimenez-Aparicio, C. A. Murillo, F. A. Urbanos, D. Villagran, X. Wang, *J. Am. Chem. Soc.* **2007**, *129*, 12666–12667.
[30] M. C. Barral, T. Gallo, S. Herrero, R. Jimenez-Aparicio, M. R. Torres, F. A. Urbanos, *Inorg. Chem.* **2006**, *45*, 3639–3647.
[31] M. C. Barral, S. Herrero, R. Jimenez-Aparicio, M. R. Torres, F. Urbanos, *Angew. Chem.* **2005**, *117*, 309–311; *Angew. Chem. Int. Ed.* **2005**, *44*, 305–307.
[32] J. M. Holland, S. A. Barrett, C. A. Kilner, M. A. Halcrow, *Inorg. Chem. Commun.* **2002**, *5*, 328–332.
[33] M. Higuchi, Y. Hitomi, H. Minami, T. Tanaka, T. Funabiki, *Inorg. Chem.* **2005**, *44*, 8810–8821.
[34] W. Kosaka, K. Nomura, K. Hashimoto, S.-i. Ohkoshi, *J. Am. Chem. Soc.* **2005**, *127*, 8590–8591.
[35] H. Ando, Y. Nakao, H. Sato, S. Sakaki, *J. Phys. Chem. A* **2007**, *111*, 5515–5522.
[36] S. Hayami, R. Moriyama, A. Shuto, Y. Maeda, K. Ohta, K. Inoue, *Inorg. Chem.* **2007**, *46*, 7692–7694.
[37] M. D. Walter, C. D. Sofield, C. H. Booth, R. A. Andersen, *Organometallics* **2009**, *28*, 2005–2019.
[38] E. Añez, S. Herrero, R. Jiménez-Aparicio, J. L. Priego, M. R. Torres, F. A. Urbanos, *Polyhedron* **2010**, *29*, 232–237.

[39] R. N. Muller, L. Vander Elst, S. Laurent, *J. Am. Chem. Soc.* **2003**, *125*, 8405–8407.
[40] M. Affronte, F. Troiani, A. Ghirri, S. Carretta, P. Santini, V. Corradini, R. Schuecker, C. Muryn, G. Timco, R. E. Winpenny, *Dalton Trans.* **2006**, 2810–2817.
[41] A. Donarini, G. Begemann, M. Grifoni, *Nano Lett.* **2009**, *9*, 2897–2902.
[42] M. C. Barral, S. Herrero, R. Jimenez-Aparicio, M. R. Torres, F. A. Urbanos, *J. Organomet. Chem.* **2008**, *693*, 1597–1604.
[43] F. A. Urbanos, M. C. Barral, R. Jiménez-Aparicio, *Polyhedron* **1988**, *7*, 2597–2600.
[44] J. O. Jensen, *THEOCHEM* **2005**, *723*, 1–8.
[45] S. Kudoh, M. Takayanagi, M. Nakata, *Chem. Phys. Lett.* **2000**, *322*, 363–370.
[46] C. J. O'Connor in *Magnetochemistry-Advances in Theory and Experimentation, Vol. 29* (Ed.: S. J. Lipper), Wiley, New York, **1982**.
[47] F. D. Cukiernik, A.-M. Giroud-Godquin, P. Maldivi, J.-C. Marchon, *Inorg. Chim. Acta* **1994**, *215*, 203–207.
[48] E. J. Beck, K. D. Drysdale, L. K. Thompson, L. Li, C. A. Murphy, M. A. S. Aquino, *Inorg. Chim. Acta* **1998**, *279*, 121–125.
[49] F. D. Cukiernik, D. Luneau, J.-C. Marchon, P. Maldivi, *Inorg. Chem.* **1998**, *37*, 3698–3704.
[50] M. C. Barral, R. Jimenez-Aparicio, D. Perez-Quintanilla, J. L. Priego, E. C. Royer, M. R. Torres, F. A. Urbanos, *Inorg. Chem.* **2000**, *39*, 65–70.
[51] C. Herrmann, J Neugebauer, J. A. Gladysz, M. Reiher, *Inorg. Chem.* **2005**, *44*, 6174–6182.
[52] G. Zhang, C. B. Musgrave, *J. Phys. Chem. A* **2007**, *111*, 1554–1561.
[53] SHELXS97, Program for Refinement of Crystal Structure, G. M. Sheldrick, University of Göttingen, Göttingen, **1997**.
[54] The reader should keep in mind that, although the comparison between the results from experimental and computationally optimised geometries can be qualitatively helpful, they cannot be rigorously considered. Therefore, the comparison of structural and energetic data between **5** and **1**–**4** should be taken only as a guideline.
[55] D. Andrae, U. Häußermann, M. Dolg, H. Stoll, H. Preuß, *Theor. Chim. Acta* **1990**, *77*, 123–141.
[56] R. Krishnan, J. S. Binkley, R. Seeger, J. A. Pople, *J. Chem. Phys.* **1980**, *72*, 650–654.
[57] P. J. Stephens, F. J. Devlin, C. F. Chabalowski, M. J. Frisch, *J. Phys. Chem.* **1994**, *98*, 11623–11627.
[58] Y. Shao, L. Fusti-Molnar, Y. Jung, J. Kussmann, C. Ochsenfeld, S. T. Brown, A. T. B. Gilbert, L. V. Slipchenko, S. V. Levchenko, D .P. O'Neill, R. A. DiStasio Jr, R. C. Lochan, T. Wang, G. J. O. Beran, N. A. Besley, J. M. Herbert, C. Y. Lin, T. Van Voorhis, S. H. Chien, A. Sodt, R. P. Steele, V. A. Rassolov, P. E. Maslen, P. P. Korambath, R. D. Adamson, B. Austin, J. Baker, E. F. C. Byrd, H. Dachsel, R. J. Doerksen, A. Dreuw, B. D. Dunietz, A. D. Dutoi, T. R. Furlani, S. R. Gwaltney, A. Heyden, S. Hirata, C.-P. Hsu, G. Kedziora, R. Z. Khalliulin, P. Klunzinger, A. M. Lee, M. S. Lee, W.-Z. Liang, I. Lotan, N. Nair, B. Peters, E. I. Proynov, P. A. Pieniazek, Y. M. Rhee, J. Ritchie, E. Rosta, C. D. Sherrill, A. C. Simmonett, J. E. Subotnik, H. L. Woodcock III, W. Zhang, A. T. Bell, A K. Chakraborty, *Phys. Chem. Chem. Phys.* **2006**, *8*, 3172–3191.

Received: December 11, 2009
Published online: April 21, 2010

